



# Novel Speckle Preparation and Heat Insulation Method for DIC Strain Measurement at Cryogenic Temperature and Large Deformation Environment

J. Yang<sup>1,2</sup> · Y. Li<sup>1,2</sup> · J. Deng<sup>1,2</sup> · Z. Zhang<sup>1,2</sup> · J. Zhou<sup>1,2</sup> · X. Zhang<sup>1,2</sup> 

Received: 24 April 2023 / Accepted: 2 October 2023 / Published online: 25 October 2023  
© Society for Experimental Mechanics 2023

## Abstract

**Background** The accuracy and reliability of digital image correlation (DIC) technologies are not only dependent on correlation algorithms but also strongly affected by the quality of the speckle patterns, especially under extremely low temperatures and large deformation conditions.

**Objective** To overcome the challenge that the speckle patterns become more brittle and harder in the extremely low temperature experiments near liquid helium, and speckles cracking and shedding during the large deformation processes.

**Methods** Novel speckle patterns and fabrication technologies have been developed specifically tailored to extremely low temperatures and large deformation conditions.

**Results** A novel spinning-coated speckle fabrication method based on PDMS silicone and TiO<sub>2</sub> spherical particles was proposed, which can enable extremely low temperatures of DIC measurements above 20% strain. Using the 316LN stainless steel as a sample, the performances of several common speckles have been compared, and the strain localization and propagation had also been clarified.

**Conclusions** The novel DIC full-field measurement method was validated with 316LN stainless steel, which confirmed that the speckles have excellent stability in the process of large deformation at extremely low temperatures. In addition, the formation and propagation processes of the slip bands for 316LN stainless steel have been revealed.

**Keywords** Digital image correlation · Extremely low temperatures · Speckle patterns · Large deformation measurement · 316LN stainless steel

## Introduction

Rapidly rising interest in the mechanical behavior of engineering materials under extremely low temperature conditions has been stimulated by the dynamic development of the cryogenic industry. Acquisition of deformation and strain measurements plays a vital role in understanding the performance of related materials and designing cryogenic

engineering applications. Although extensometers have been utilized extensively in cryogenic and large deformation load frame design, they have been gradually replaced by more advanced digital image correlation (DIC) technology in many experiments, due to their contact, uniaxial, and local average response limitations. DIC technology, first developed in the 1980s [1, 2], has been widely used for shape, motion, and deformation measurement in a variety of observation scales and special environments [3, 4]. After continuous improvement, this method has already owned many incomparable advantages, including a simple device, easy realization, full field *in-situ* observation, strong robustness to environmental vibration and light changes, wide application range, and adjustable spatial-temporal resolution. The speckle pattern, a random feature pattern on the sample, plays the role of deformation information carrier in DIC measurements. In recent years, numerous studies have shown that the accuracy and precision of DIC measurement

✉ X. Zhang  
zhangxingyi@lzu.edu.cn

<sup>1</sup> Key Laboratory of Mechanics on Disaster and Environment in Western China attached to the Ministry of Education of China, Lanzhou University, Lanzhou, Gansu 730000, China

<sup>2</sup> Department of Mechanics and Engineering Sciences, College of Civil Engineering and Mechanics, Lanzhou University, Lanzhou, Gansu 730000, China

strongly depend on the quality of speckle pattern and the associated algorithms [5–7]. Considering the huge diversity of material category, observation space scales and temperature environment, speckle pattern fabrication and its quality usually serve as the decisive conditions for the application of DIC technology in a specific experiment.

The speckle patterns mainly include two types: natural texture speckles and manufactured speckles. The former is a material inherent microstructure. Compared with manufactured patterns, it is often difficult to realize DIC measurement due to its insufficient information carriers or low pattern quality [8]. As a result, natural speckle is only employed in some micro-scale measurements, and its application field is relatively limited. Manufactured speckle mainly includes spraying speckles, spraying white or black speckles on the sample surface with a spray bottle or gun [3, 9], spin coating, preparing a mixture of suitable proportions, and then obtaining the ideal speckle coating by depositing, rotating, and evaporation steps [10, 11]. Additionally, manufactured methods also include lithography, nano-film remodeling, compressed air technique, etc. These speckle fabrication technologies can meet the test requirements of most conventional experiments. Nevertheless, special treatment and improvements are often required for unusual situations, especially at extreme temperatures.

The effective temperature of the speckle pattern, self-illumination, and thermal radiation-induced speckle pattern inversion are the primary challenges for DIC measurements at high temperatures. To address these issues, Thai et al. sprayed a high-temperature-resistant white pattern on marble slabs and extruded graphite rods. They achieved DIC strain observation above 1000°C by isolating reflection speckle spectra [12] and adjusting camera exposure time [13], respectively. Furthermore, using a blue light band-pass filter and alumina paints, Wang et al. have achieved full-field strain mapping for a C/C composite tensile specimen at 2000°C. Eventually, in Pan's work, their TaC speckle pattern and narrow-band filtering method have helped them to successfully perform DIC measurement at 3000°C [14]. It can be concluded that extensive research has been conducted on speckle fabrication, digital signal acquisition, and post-processing technologies for high-temperature DIC experiments.

On the contrary, since most materials will become more brittle and harder at extremely low temperatures, this change could directly restrict the strain available range of speckle patterns in some cryogenic experiments. For instance, the fracture elongation of some commonly used stainless steel materials has exceeded 20% in cryogenic environments, including 304 [15], 316LN [16], and some high entropy alloys [17]. As a result, the speckle must have a greater strain-bearing capacity than the sample itself to accurately capture strain distribution during massive deformation. Fortunately, Wu et al. have analyzed the micro-scale to macro-scale deformation responses

of the FeMnNiCoCr high entropy alloy and explained its exceptional strain hardening behavior at 77 K with the DIC measurements [18]. However, their speckle patterns are made by the scratching/abrading method, and additional polishing is required for each load increment to ensure the speckle quality. Similarly, Wilson et al. have also used the polishing method for their speckle fabricating at –100°C [19], while their strain measurement range is relatively small. Additionally, at liquid nitrogen temperature, randomly spray-painted black/white speckles on the sample faces were also applied [20, 21]. However, there have been no detailed studies on optimizing the preparation and assessing speckle quality for large deformation measurements at liquid nitrogen or even helium temperatures.

In this paper, to solve the shedding and cracking problems of speckles themselves at cryogenic temperatures and large deformation environment, we proposed a novel spinning coated speckle fabrication method based on PDMS (Polydimethylsiloxane) silicone and TiO<sub>2</sub> spherical particles mixed solution, its stability was verified in the low temperature DIC strain measurement. In addition, considering that the specific heat of the material tends to zero in the ultra-low temperature environment, any small external heat input will lead to a sharp temperature increase in the sample [22, 23]. As shown in the following equations, the heat increment  $Q$  is related to temperature  $T$  by

$$dQ = mCdT. \quad (1)$$

Where the  $m$  is the mass of the sample, and it can be transformed to

$$\frac{dT}{dQ} = \frac{1}{mC}. \quad (2)$$

Knowing that  $C \rightarrow 0$  when  $T \rightarrow 0$ , we have

$$\frac{dT}{dQ} \rightarrow \infty. \quad (3)$$

Thus, a set of heat-insulating polarized light paths was proposed to lessen the impact of thermal radiation from external light on the sample. Finally, choosing the 316LN stainless steel (fracture elongation more than 25% at 20 K) as the experimental sample, we compared the performance of several commonly available speckles and our self-made PDMS-TiO<sub>2</sub> speckle at different deformation stages and measured their strain applicable range at room and low temperatures.

## Methodology

### Fabrication of Speckle Patterns

Because of its excellent temperature resistance and flexibility, PDMS silicone rubber is widely used in the aircraft

and electronic packaging field [24–26]. The low viscosity of PDMS, before it solidifies, makes it a good candidate for doping with other hard particles to create a mixed liquor. After spinning coating and baking, the volume of silicone rubber reduces and will solidify on the sample surface. At the same time, the white particles will distribute on the sample surface randomly, and the particles adhere to the sample by the solidified silicone rubber around them, as shown in Fig. 1(a). Since the PDMS silicone rubber itself has a high light transmission (more than 99%), it is essentially undetectable in the light path, leaving only sporadic white dots visible on the sample's surface. On the other hand, the  $\text{TiO}_2$  spherical particles are tough and small (50–80  $\mu\text{m}$  in diameter), so they are almost impossible to break. Finally, with the adhesion and fixation effect of rubber, this method can address the issues of cracking and shedding of speckle patterns at low temperatures. The specific preparation process is shown in Fig. 1(b).

To create the speckle mixture, PDMS silicone rubber liquid, curing agent (hydrogen-containing polydimethylsiloxane),

and  $\text{TiO}_2$  spherical particles are combined in specific mass ratios of 45%, 5%, and 50%, respectively. The proportion of the curing agent mainly affects the solidification time and hardness of the speckle mixture. If too little curing agent is used, the solidification time of the entire mixture will be too long or even not solidified. Inversely, the final solidified silicone rubber will be hard and have poor adhesion. Under this proportion, the solidification time of the mixed solution is about 30–50 min, which can meet the time of the spin coating process, and the entire solidification process can occur in the vacuum baking process.

Because the  $\text{TiO}_2$  particles hardly deform, this speckle pattern only reflects the sample deformation by the relative position change between different particles. This is indeed a limitation of this method compared to other speckles. For the  $\text{TiO}_2$  particles, one should choose the smallest possible particles that can be recognized based on the spatial resolution of the camera, to obtain a better “strain spatial resolution”, especially for some experiment that aims to observe local strain distribution. After the particle size is fixed, different

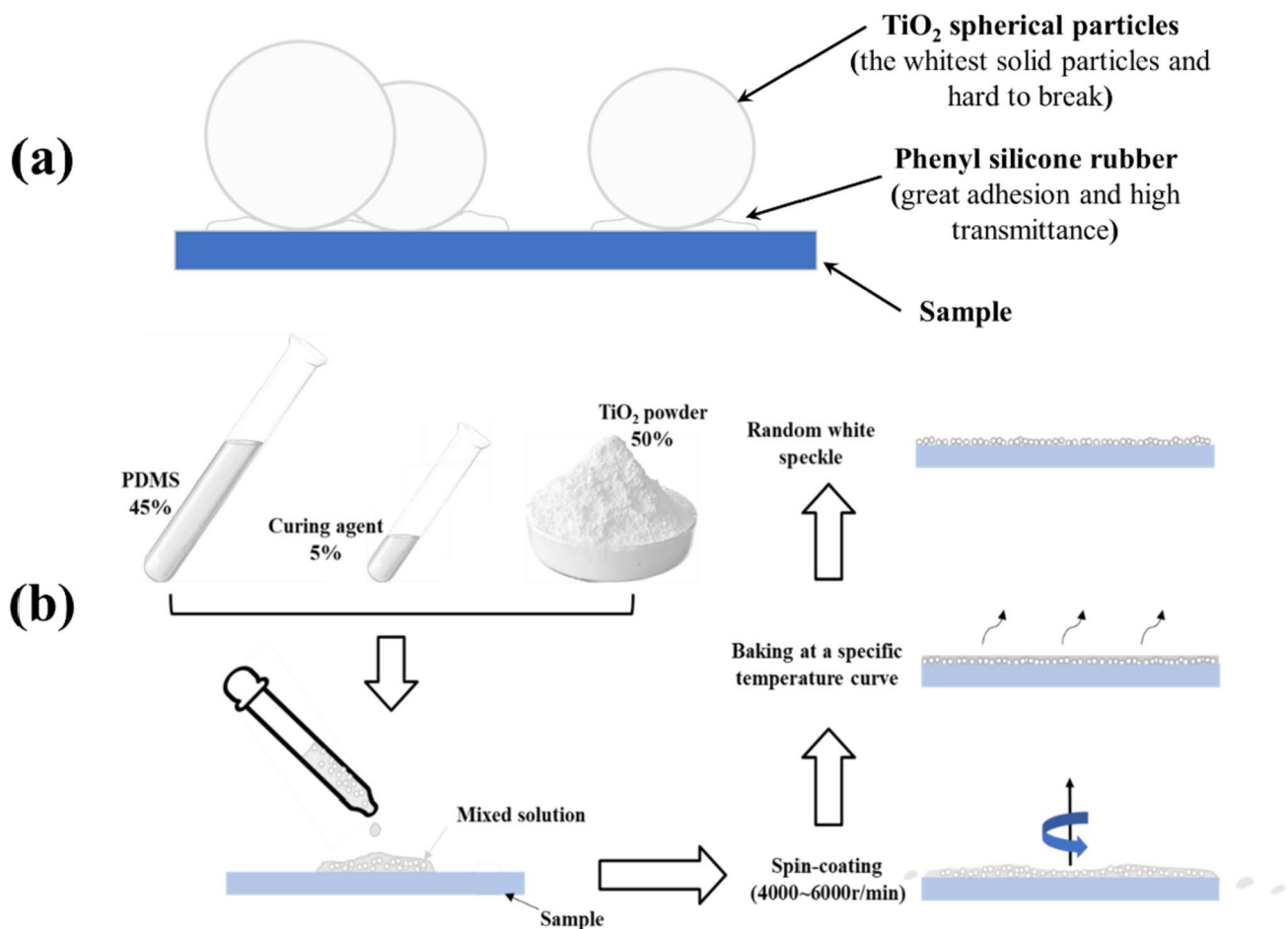


**Fig. 1** (a) Schematic diagram of the spherical particles adhered to the sample surface by PDMS, and (b) the fabricating processes of the PDMS- $\text{TiO}_2$  speckle patterns

mass fractions only affect the number of particles. In this work, relatively high particle mass fractions were used, which can provide more information to meet the DIC strain calculation. However, it should be noted that if the particle mass fraction is too high, more aggregation between particles will be formed, also resulting in poor speckle quality.

After thorough mixing, the mixture is placed in a vacuum chamber to eliminate any air bubbles, and to avoid the uneven particle distribution caused by local bubbles. By spinning the prepared speckle mixture with a rotation speed of 6000 r/min for 6 min, a satisfactory uniform particle distribution can be obtained. The rotation speed and duration of the spin coating should be adjusted based on the concentration of the mixture and sample size. After baking at specified temperatures (raise from room temperature to 120°C at a speed of 2°C/min, then keep it for 2 h, and finally return to room temperature naturally), the desired random speckle patterns can be achieved, as shown in Fig. 2. For the speckle pattern coating obtained by the above processes, the topography of the junction between the PDMS film and 316LN sample surface was scanned by AFM. The thickness of the coated PDMS film is about 8.54  $\mu\text{m}$ , and the thickest part at the edges is about 10  $\mu\text{m}$ .

### System Components and Experiment Method

The optical path diagram in Fig. 3 illustrates the components of the system, which include an LED light source, heat insulation glass, polarizer, analyzer, and camera. In this experiment, the white light from the LED light source will pass through a heat insulation glass and it's then collimated and linearly polarized by a polarizer. Subsequently, the polarized light beam directly passes through the K9 glass window of the cryogenic loading device and is reflected after reaching the sample surface. The reflected light from the sample and speckle surface passes through an analyzer before being imaged by a camera. The cryogenic loading system provides

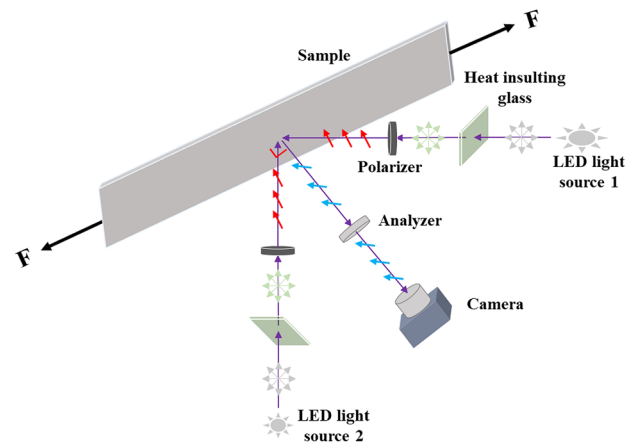


Fig. 3 Schematic diagram of the heat-insulating polarized optical path

the loading and cooling conditions, and its detailed parameters are described in the reference [27].

The purpose of using heat insulation glass is to reduce the heat radiation from the external light by filtering out the light with wavelengths greater than 650 nm. After the light is filtered by the polarizer, the thermal radiation could also be reduced, and this is the first purpose of using the polarized path. More importantly, by adjusting the analyzer angle during the image acquisition process, most stray light and the influence of specular reflection from the sample surface can be effectively eliminated, which will significantly improve the signal-to-noise ratio of the image. Figure 4 illustrates the effect of improving the image quality by adjusting the analyzer angle. Of course, the absolute orthogonal state is not recommended in the experiment, because at this state, higher light power or much longer exposure time is needed to meet the normal shooting requirements.

Figure 5 compares the radiation heating effects of different light paths using the same camera parameters and obtaining the same speckle pattern brightness. The results show

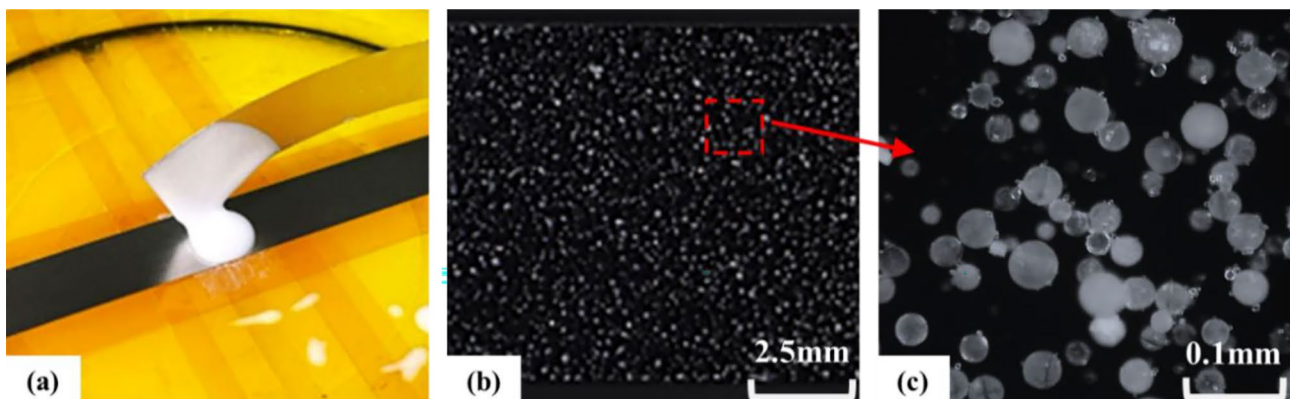
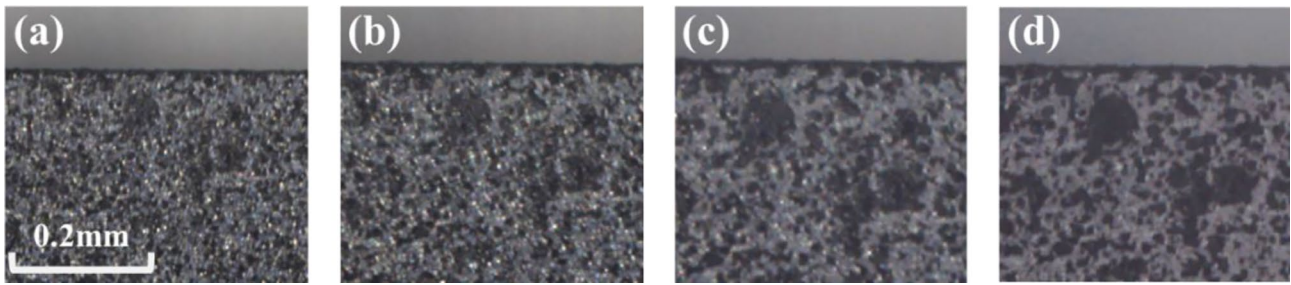


Fig. 2 (a) Speckle preparation mixture, (b) the final speckle coated on the 316LN sample surface, and (c) its local enlarged view





**Fig. 4** Speckle pattern images were acquired with various analyzer angles of (a) 0°, (b) 30°, (c) 60°, and (d) 90°, respectively

that the LED polarized insulation light path has the least radiation heating influence on the sample, and the sample temperature only rises by about 2 K. In contrast, fluorescent light has a more noticeable thermal radiation heating effect compared with LED.

The duty ratio (proportion of the speckle pattern area to the total selected area) of PDMS-TiO<sub>2</sub> speckle is 16.46%, which is calculated from Fig. 6(b) binary image. The speckle diameter is measured to be 10.27 pixels, and the autocorrelation coefficient curve and surface diagram result calculated with a 41 × 41 pixels subarea were also shown in Fig. 6(c), (d). Moreover, the simple yet effective global parameter, mean intensity gradient (MIG) proposed by Pan et al. was chosen to evaluate the quality of the various speckle patterns [28]. From the results in Table 1, it can be seen that the MIG of hydrographic printing and UV printing speckles are still much higher than other speckles. This kind of speckle pattern pre-designed by the software can meet a higher MIG through the adjustment of the design process. PDMS-TiO<sub>2</sub> speckle, spraying paint, and fluorescent speckle perform similarly on MIG.

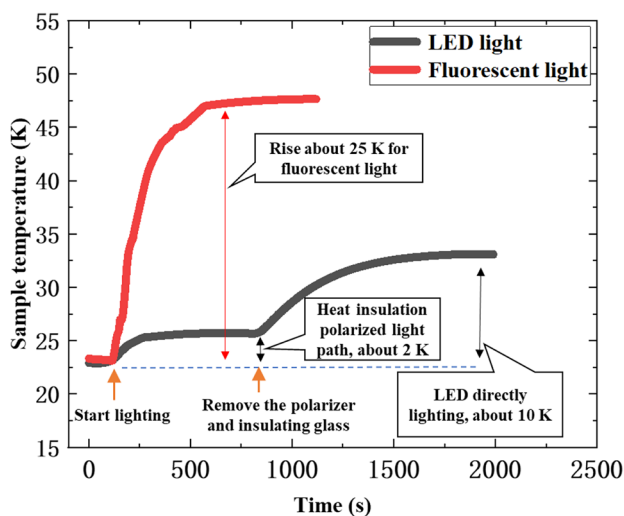


**Fig. 5** Radiation heating effects of LED and fluorescent light path

### Experimental Samples and Parameters

In this work, 316LN stainless steel was chosen as the tensile test sample for DIC measurements. Depending on its excellent mechanical properties and corrosion resistance at low temperatures, 316LN is widely used in various cryogenic industrial and new large science facilities. As can be seen from the macroscopic stress-strain curve in Fig. 7, the fracture elongation of 316LN has exceeded 20% at both room and low temperatures, and its strength has been significantly improved at 20 K. It should be noted that the stress jump in the plastic stage at 20 K is a kind of discontinuous serrated-plastic-yielding behavior of 316LN. Relevant mechanical mechanisms and calculating models are introduced [22, 29–31], and this behavior does not belong to accidental phenomena or experimental errors.

Paints spraying (without substrate layer), UV printing, hydrographic printing, fluorescent spraying [32], four kinds of commonly used speckles, and the aforementioned PDMS-TiO<sub>2</sub> speckle were prepared on the sample surface and the diameter of all speckles was controlled at about 60–100 microns. Then the painted 316LN samples (10 mm × 120 mm × 0.1 mm) will be loaded at 300 K and 20 K at the same loading strain rate of  $2.7 \times 10^{-3}$ /s. For each set of loading experiments, a thermocouple thermometer was pasted on the back of the samples to monitor the temperatures. On the other hand, the fluorescent speckle was directly illuminated by a specific light source with a wavelength of about 365 nm, so the external heat insulation filter element is no longer applicable at this time. In addition, other samples were tested in the LED heat insulation polarized optical path.

The camera exposure time is fixed at 80 ms for various speckle patterns, and the capture frame rate is one frame per second. For different speckle patterns, after fixing the camera parameters, the power of the LED or fluorescent light source was adjusted to make the gray level difference between the bright and dark regions of the final captured images around 220 (0–255 Gray level range). In the DIC calculation process, every speckle pattern group uses the same parameter settings. The diameter of the image

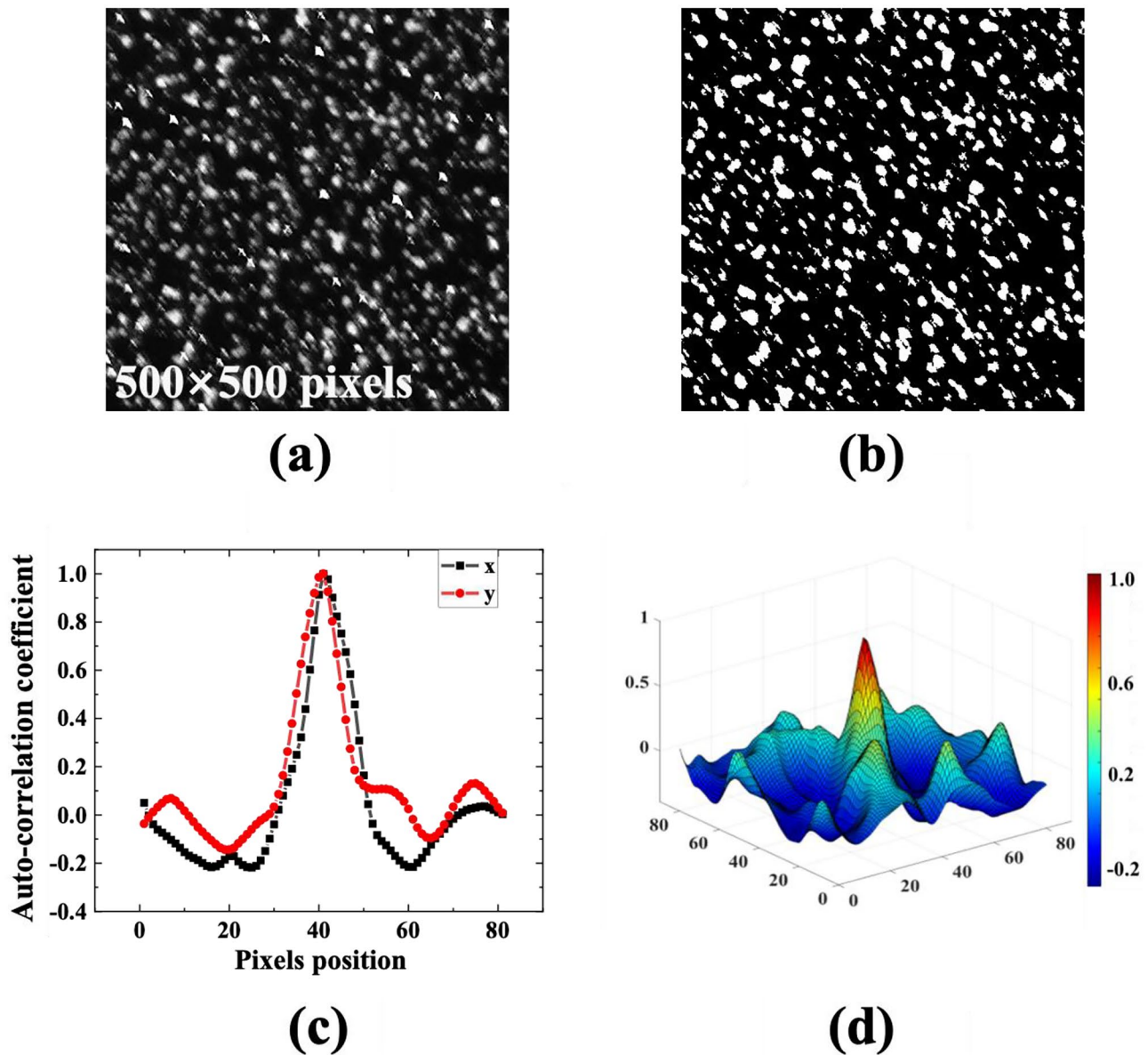


**Fig. 6** Quality evaluation for the PDMS-TiO<sub>2</sub> speckles. (a) the speckle pattern image acquired at 20 K before deformation and (b) its binary image with a threshold of 86, the auto-correlation coefficient curve (c) and surface diagram result (d) calculated with a subarea of 41 × 41 pixels

matching sub-region and strain calculation sub-region was 41 and 21 pixels, respectively. At the same time, the calculation step size for each speckle pattern is 1 pixel.

**Table 1** Mean image intensity gradient of each speckle pattern calculated with a subarea of 500 × 500 pixels

Speckle pattern	Black spray paint	UV printing	Hydrographics printing	Fluorescent printing	PDMS-TiO <sub>2</sub> speckle
MIG	29.55	46.81	48.52	27.28	28.228

## Results and Discussion

### Performance of Various Speckle Patterns

Figures 8 and 9 show the performance of several selected speckles during the deformation processes at both room and low temperatures. For each sample, five strain (engineering strain) observation points of  $\epsilon = 0\%$  (initial state),  $\epsilon = 1\%$ ,  $\epsilon = 5\%$ ,  $\epsilon = 10\%$ , and  $\epsilon = 20\%$  were chosen to monitor the speckle pattern state. Except for Fig. 8(b), on the right side of the colour bar for each set of results, the enlarged images of the local speckle under the corresponding strain have

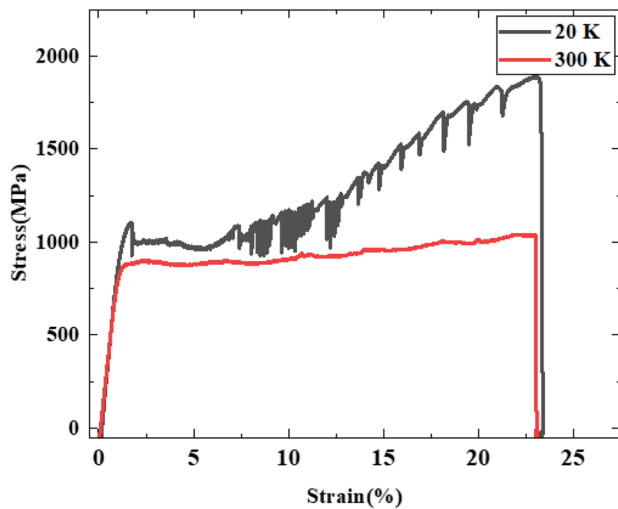


**Fig. 7** Stress-strain curves of 316LN stainless steel with temperatures of 20 K and 300 K

been shown. Comparing the results of each group, the relevant results can be obtained as follows

1. All of the samples maintain a non-uniform strain distribution during the entire deformation process at both room and low temperatures, and the mechanism of strain propagation was found to be similar for each sample. Firstly, after the total strain reaches about 2%, the strain at both temperatures localizes in the form of cross-slip bands and then spreads throughout the entire observation area along the loading direction. Furthermore, during the significant deformation plastic stage, the local strain differential can exceed 10%. This result also emphasizes the importance and necessity of full field and *in-situ* measurements.
2. For the DIC experiment at 300 K, spraying paint, fluorescent, and self-made PDMS-TiO<sub>2</sub> speckle patterns can meet the strain observation requirements of more than 20%. The strain available range of hydrographic printing and UV printing speckle is about 7%, beyond which the speckle itself will crack.
3. For the DIC experiment conducted at 20 K, we found that the spraying black speckle was able to remain stable in the elastic stage. However, when the total strain reached 5%, the speckle itself cracked due to its poor strain-bearing capacity at low temperatures, as shown in Fig. 8(b). Additionally, due to hardening and poor adhesion at low temperatures, the shedding of speckles also occurred, as shown in Fig. 8(b). These two factors led to more areas failing to match (the black defect area in the strain cloud map) during the calculation process, thereby increasing the error of the strain results. Finally, when the strain reached 20%, it was difficult to achieve region

pattern matching and calculate the strain distribution in most areas. Similarly, both hydrographic printing and UV printing speckles cracked when the strain exceeds 1%, failing pattern matching in most areas. In comparison, homemade and fluorescent speckles exhibited the most stable performance, as they did not crack or shed during the entire deformation process.

4. Furthermore, we found that the thermal radiation of the fluorescent light path was higher than that of the LED. However, the insulation polarized light path combined with the PDMS-TiO<sub>2</sub> speckle was able to achieve DIC measurements of over 20% strain with minimal impact on the low-temperature environment of the sample.

### Slip Band Evolution

In the overall mean strain range of 4% to 8%, the evolution process of the slip band is depicted in Fig. 10(a). At the same strain increment of  $\Delta\varepsilon = 0.04$ , the slip band propagation displacement  $\Delta X_1$  and  $\Delta X_2$  at 300 K and 20 K is 20.89 mm and 19.61 mm, respectively, indicating that the expansion velocity of the slip band is almost unaffected by the low-temperature environment at the same loading rate.

Additionally, to observe the formation and evolution process of the slip band more clearly, the photos when the sample is deformed to about 2% average strain, are selected as the reference image for calculation. This method can eliminate the “background strain” of the sample deformed in the early stage, allowing for better observation of the slip band during a smaller strain interval. As can be seen from the results in Fig. 10(b) the local strain of a new slip band gradually increases to about 8.8% and then remains stable. At the same time, other new slip bands also form in nearby regions. The larger strain areas of both room and low temperature samples localize at the intersection of the slip bands. However, for the results at room temperature, the phenomenon of local strain concentration is more pronounced. The selected central rhomboid area has an average strain of roughly 8.5%, whereas the equivalent region in the 20 K sample has a strain of 7.6%. It is noteworthy that the plastic flow stress for the slip band expansion process is 880–900 MPa at 300 K, whereas the stress at 20 K exceeds 1000 MPa, and it would even exceed 1500 MPa at the later slip band propagation stage. This is because the phase transformation driving force of such metastable austenitic stainless steel decreases at a cryogenic temperature environment, and most austenitic parent phase gradually transforms into a martensitic phase during the loading process. Moreover, the nucleation of the martensitic phase often occurs at the intersection of the slip bands [33]. With the accumulation of plastic strain, more martensite forms, and more stress will



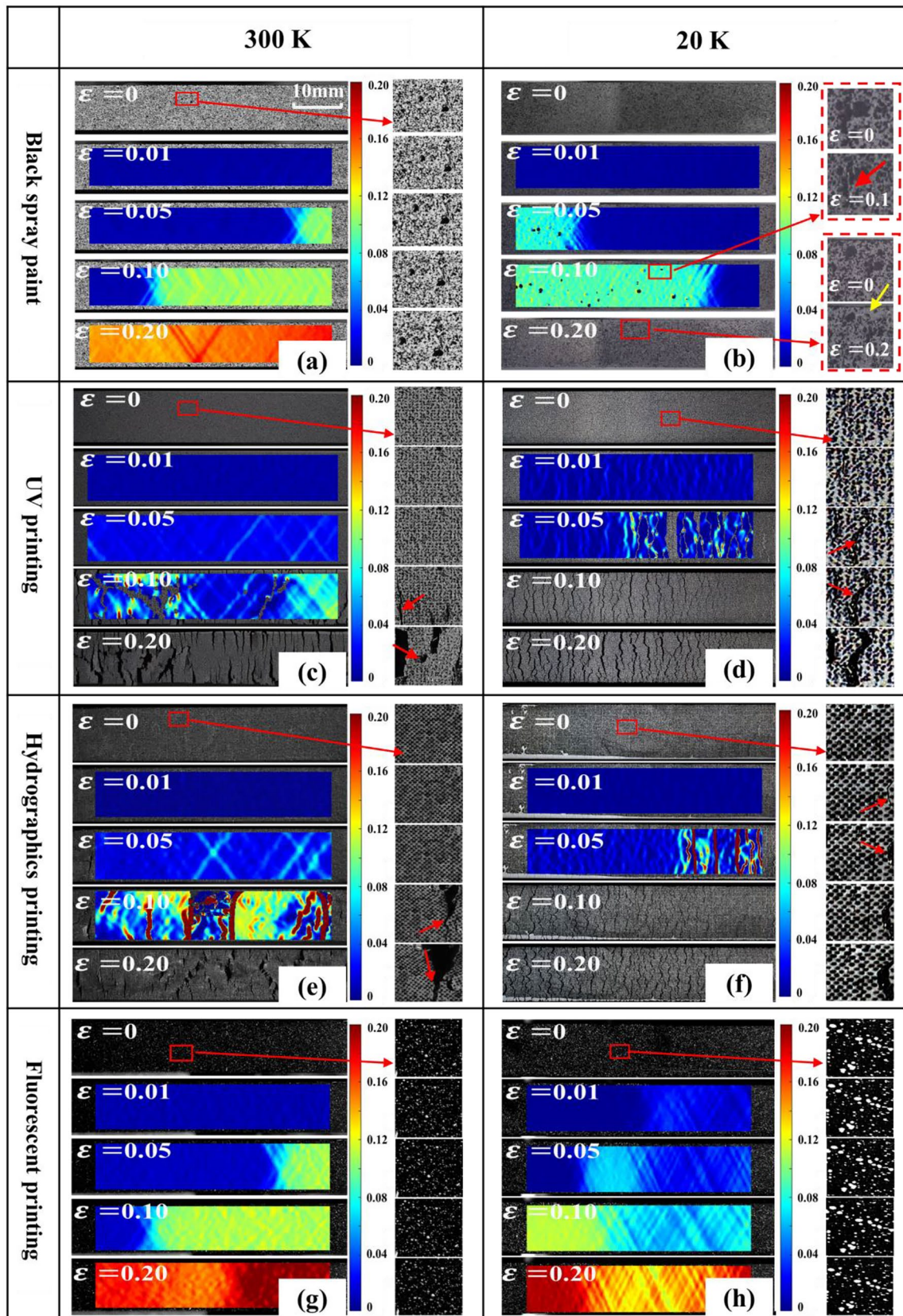


**Fig. 8** The performance of selected speckles with various strains at both room and low temperatures, (a) and (b) black spraying point, (a) and (d) UV printing, (e) and (f) hydrographic printing, (g) and (h) fluorescent speckles with the temperature of 300 K and 20 K, where the red and yellow arrowheads mark the fracture and fall off positions, respectively



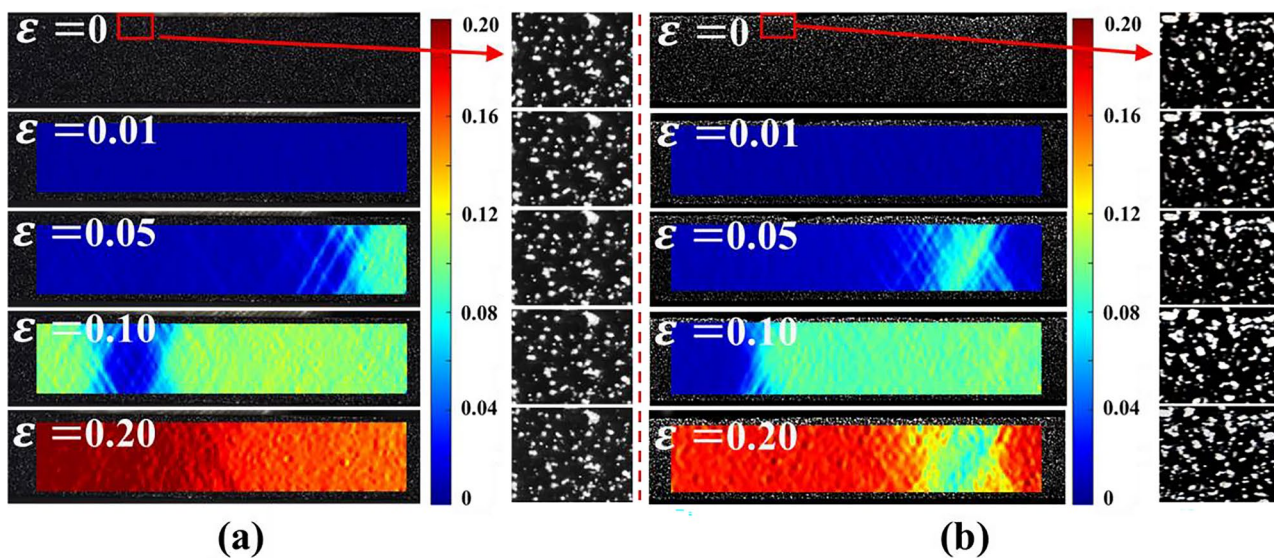


Fig. 9 Performance of PDMS-TiO<sub>2</sub> speckle with the temperature of (a) 300 K and (b) 20 K

be borne by martensite in the low-temperature sample. As a strengthening phase, martensite has a higher modulus and temperature dependence than that of austenite at low temperatures, making the low temperature strain concentration

area in Fig. 10 capable of withstanding higher stress at a smaller strain.

As both temperature reduction and plastic strain augment can facilitate the transformation of austenite to martensite in

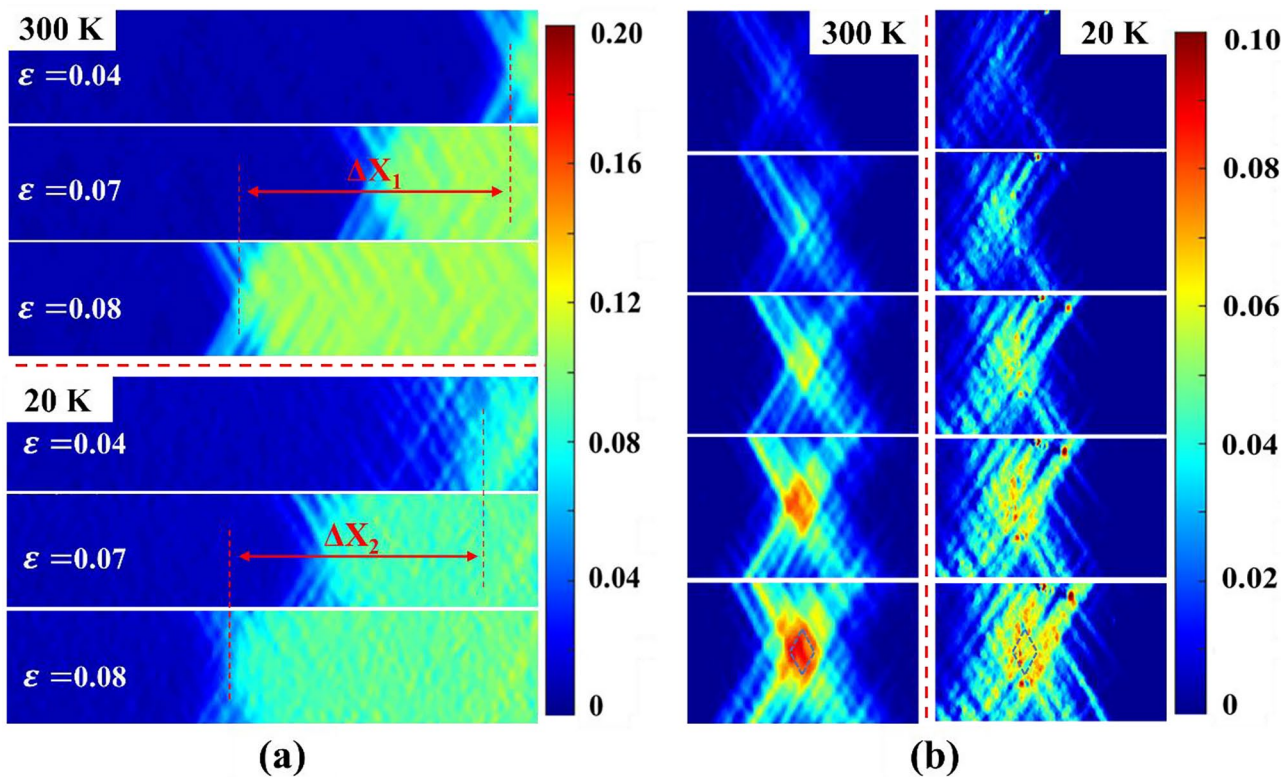
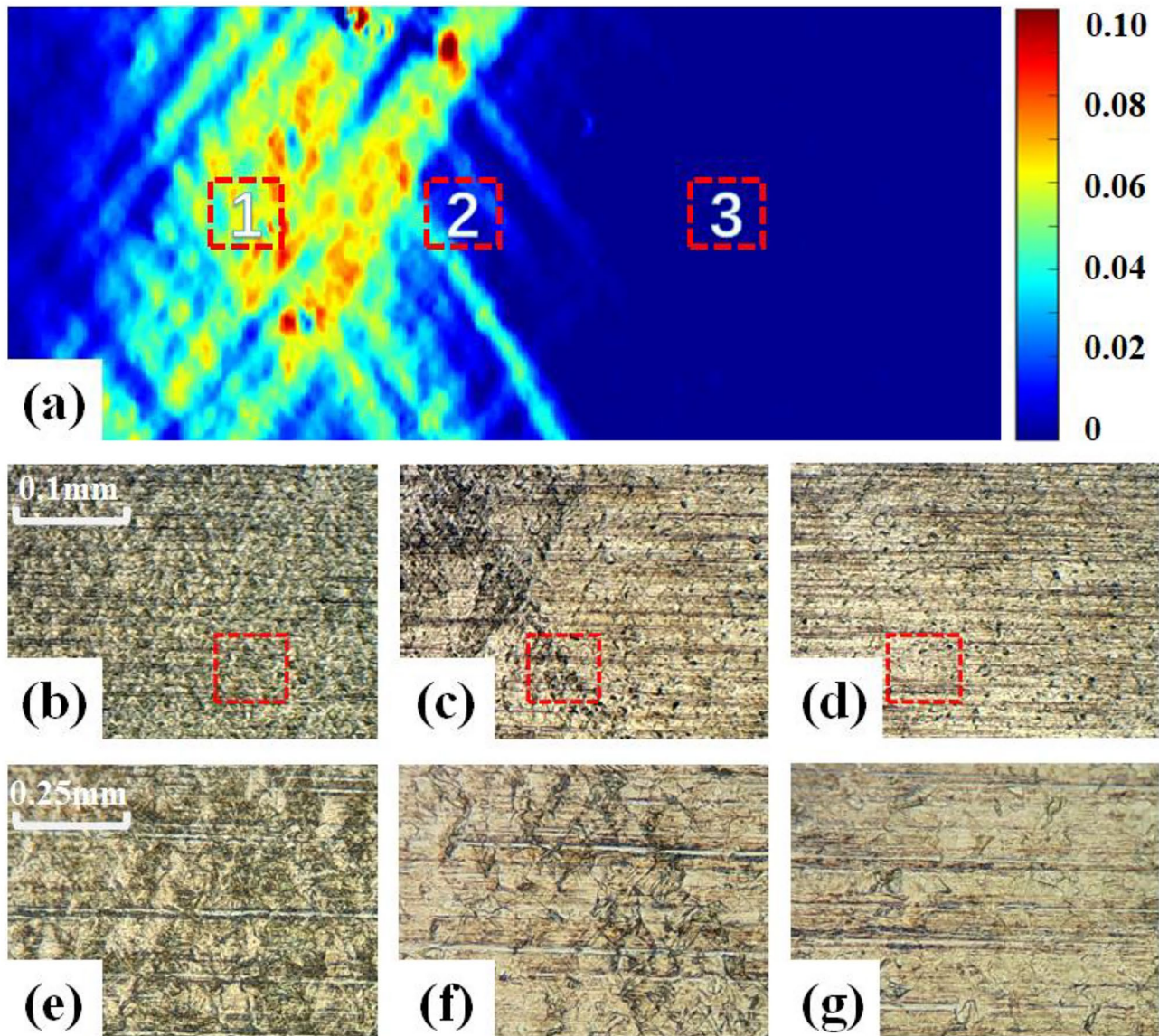


Fig. 10 (a) Propagation process of the slip band during the full-field strain at 4% to 8% with the temperature of 300 K and 20 K. (b) Evolution of slip band with the strain increment of 0.13% with the temperature of 300 K and 20 K





**Fig. 11** (a) The DIC results of propagation of slip bands for 316LN stainless steel, (b)–(g) the metallographic microscope observation results, among them, figures (b)–(d) correspond to positions 1–3 marked in figure (a), respectively, figures (e)–(g) are local enlarged views of the red rectangles in figures (b)–(d)

316LN stainless steel. The sample of Fig. 10(b) with locally formed slip bands at 20 K was unloaded and heated back to room temperature to investigate the phase transformation during slip band extension. After thorough polishing, three regions shown in Fig. 11 were selected for metallographic observation: 1) the area where slip bands propagated, 2) the boundary of slip band extension, 3) the area where no slip bands were generated. Figure 11 revealed that as slip bands propagated, the originally yellow-white austenite phase in 316LN gradually transformed into a black-green martensite phase. Notably, the boundary of slip bands in regions (c) and (f) served as the main nucleation and growth region of martensite phase transformation.

## Conclusions

In this work, a novel spinning-coated speckle fabrication method based on PDMS (Polydimethylsiloxane) silicone and  $\text{TiO}_2$  spherical particles was proposed, which can enable extremely low temperatures DIC measurements above 20% strain with less radiation heating effect on the sample combined with a heat-insulating polarized light path. Moreover, using the 316LN stainless steel as a sample, we have performed *in-situ* DIC measurements of several commonly available speckles and our self-made PDMS- $\text{TiO}_2$  speckle at both room and cryogenic temperatures. Finally, the experimental results verified that our speckle has excellent stability

during the large deformation process at low temperatures. In addition, the formation and evolution processes of the slip band for 316LN stainless steel are also discussed.

**Acknowledgements** The authors thank Prof. X. X. Shao (South-east University, China) and Prof. Z. N. Chen (Nanjing University of Aeronautics and Astronautics, China) for their help at the fabrication method of DIC speckle for room temperature measurement and critical discussion. This work was supported by the National Natural Science Foundation of China (Nos. 12232005, U2241267).

**Funding** National Natural Science Foundation of China, 12232005, U2241267.

**Data Availability** The data that support the findings of this study are available from the corresponding author upon reasonable request.

## Declarations

**Competing Interest** The authors declare no conflicts of interest.

## References

- Peters W, Ranson W (1982) Digital imaging techniques in experimental stress analysis. *Opt Eng* 21:427–431
- Chu T, Ranson W, Sutton MA (1985) Applications of digital-image-correlation techniques to experimental mechanics. *Exp Mech* 25:232–244
- Pan B, Qian K, Xie H, Asundi A (2009) Two-dimensional digital image correlation for in-plane displacement and strain measurement: a review. *Meas Sci Technol* 20:062001
- Pan B (2010) Recent progress in digital image correlation. *Exp Mech* 51:1223–1235
- Dong YL, Pan B (2017) A review of speckle pattern fabrication and assessment for digital image correlation. *Exp Mech* 57:1161–1181
- Zhou P (2001) Subpixel displacement and deformation gradient measurement using digital image/speckle correlation (DISC). *Opt Eng* 40:1613–1620
- Lecompte D, Smits A, Bossuyt S, Sol H, Vantomme J, Van Hemelrijck D et al (2006) Quality assessment of speckle patterns for digital image correlation. *Opt Lasers Eng* 44:1132–1145
- Rae PJ, Palmer SJP, Goldrein HT, Lewis AL, Field JE (2004) White-light digital image cross-correlation (DICCC) analysis of the deformation of composite materials with random microstructure. *Opt Lasers Eng* 41:635–648
- Sutton MA, Orteu JJ, Schreier H (2009) Image correlation for shape, motion and deformation measurements: basic concepts, theory and applications. Springer Science & Business Media
- Wang H, Xie H, Li Y, Zhu J (2012) Fabrication of micro-scale speckle pattern and its applications for deformation measurement. *Meas Sci Technol* 23:035402
- Tyona MD (2013) A theoretical study on spin coating technique. *Adv Mater Res* 2:195–208
- Thai TQ, Ruesch J, Gradl PR, Truscott TT, Berke RB (2021) Speckle pattern inversion in high temperature DIC measurement. *Exp Tech* 46:239–247
- Thai TQ, Smith AJ, Rowley RJ, Gradl PR, Berke RB (2020) Change of exposure time mid-test in high temperature DIC measurement. *Meas Sci Technol* 31:075402
- Pan Z, Huang S, Su Y, Qiao M, Zhang Q (2020) Strain field measurements over 3000 °C using 3D-Digital image correlation. *Opt Lasers Eng* 127:105942
- Zheng C, Yu W (2018) Effect of low-temperature on mechanical behavior for an AISI 304 austenitic stainless steel. *Mater Sci Eng A* 710:359–365
- Qin J, Dai C, Liao G, Wu Y, Zhu X, Huang C et al (2014) Tensile test of SS 316LN jacket with different conditions. *Cryogenics* 64:16–20
- Naeem M, He H, Zhang F, Huang H, Harjo S, Kawasaki T et al (2020) Cooperative deformation in high-entropy alloys at ultralow temperatures. *Sci Adv* 6:eaax4002
- Wu Y, Bönisch M, Alkan S, Abuzaid W, Sehitoglu H (2018) Experimental determination of latent hardening coefficients in FeMnNiCoCr. *Int J Plast* 105:239–260
- Wilson PR, Cinar AF, Mostafavi M, Meredith J (2018) Temperature driven failure of carbon epoxy composites – A quantitative full-field study. *Compos Sci Technol* 155:33–40
- Yuan S, Cheng W, Liu W (2021) Cryogenic formability of a solution-treated aluminum alloy sheet at low temperatures. *J Mater Process Technol* 298:117295
- Cong Y, Zhai C, Sun Y, Xu J, Tang W, Zheng Y (2021) Visualized study on the mechanism of temperature effect on coal during liquid nitrogen cold shock. *Appl Therm Eng* 194:116988
- Skoczni B, Bielski J, Sgobba S, Marcinek D (2010) Constitutive model of discontinuous plastic flow at cryogenic temperatures. *Int J Plast* 26:1659–1679
- Ekin J (2006) Experimental techniques for low-temperature measurements: cryostat design, material properties and superconductor critical-current testing. Oxford University Press
- Lötters JC, Olthuis W, Veltink PH, Bergveld P (1997) The mechanical properties of the rubber elastic polymer polydimethylsiloxane for sensor applications. *J Micromech Microeng* 7:145
- Chu Z (1996) Flexible package for a tactile sensor array. Proceedings of 1996 National Sensor Conference. Delft University Press, Delft, pp 121–124
- Arquint P, Van der Wal P, van der Schoot BH, de Rooij NF (1995) Flexible polysiloxane interconnection between two substrates for microsystem assembly. Proceedings of the International Solid-State Sensors and Actuators Conference-TRANSDUCERS '95. IEEE, pp 263–264
- Yang J, Li J, Liu W, Li Y, Huang Y, Zhou J et al (2022) Development of a load frame for neutron diffraction and fluorescent thermometry at cryogenic temperature. *Rev Sci Instrum* 93:073904
- Pan B, Lu Z, Xie H (2010) Mean intensity gradient: An effective global parameter for quality assessment of the speckle patterns used in digital image correlation. *Opt Lasers Eng* 48:469–477
- Tabin J, Skoczen B, Bielski J (2016) Strain localization during discontinuous plastic flow at extremely low temperatures. *Int J Solids Struct* 97–98:593–612
- Xin J, Fang C, Huang C, Song Y, Wei J, Li L (2018) Correlation between microstructure evolution and cryogenic fracture toughness in aging ITER-grade 316LN weldments. *Cryogenics* 96:144–150
- Sitko M, Skoczni B, Wróblewski A (2010) FCC–BCC phase transformation in rectangular beams subjected to plastic straining at cryogenic temperatures. *Int J Mech Sci* 52:993–1007
- Chen Z, Tang X, Xu Y, Shao X, Sun W, He X (2022) Internal displacement measurements based on color fluorescent speckle pattern by multispectral stereo-DIC and refractive index correction. *Appl Opt* 61:6504–6509



33. Spencer K, Embury JD, Conlon KT, Véron M, Bréchet Y (2004) Strengthening via the formation of strain-induced martensite in stainless steels. *Mater Sci Eng A* 387–389:873–881

**Publisher's Note** Springer Nature remains neutral with regard to jurisdictional claims in published maps and institutional affiliations.

Springer Nature or its licensor (e.g. a society or other partner) holds exclusive rights to this article under a publishing agreement with the author(s) or other rightsholder(s); author self-archiving of the accepted manuscript version of this article is solely governed by the terms of such publishing agreement and applicable law.